Chapter 11
Nanotechnology for Detection of Small Mass Difference

11.1 Introduction

Mostly, mass of a macroscopic object is determined by comparing the gravitational forces experienced by the object and the body of known mass. Relative uncertainty in 1 kg is pretty small say one part in 10^9. However, gravitational force of an object of molecular scale is too feeble to detect. Hence, normal method of using a balance will not do for mass measurement on the microscopic scale. Measurement of mass at the microscopic scale is very vital as it serves powerful tool that can provide information about the molecular and atomic composition of an object, detection, prevention and treatment of various diseases. Mechanical balances with electronic devices can detect only up to $0.1\,\mu g$. An alternate method to measure the mass of an object is to consider mass as quantification of inertia. This principle is used in mass spectroscopy. In this the trajectory of an ionised particle in a strong electromagnetic field provides a precise measure of the inertia of the particle and hence a measure of its mass. Mass spectroscopy is able to distinguish ionised particles that differ by a single atomic mass unit. One atomic mass unit is equal to 1.66×10^{-27} kg. However, mass spectroscopy is restricted to ionised particles so it cannot be applied to all microscopic objects, which are neither in charged state nor can be charged. So for smaller masses, one has to depend upon certain other phenomenon.

For quite some time, many researchers were pondering whether a less complex and more versatile technique could be devised that has a microscopic sensitivity.

11.2 Cantilever Vibration

Vibration is the most common phenomenon, which everybody comes across. Vibrating of object is an inertial phenomenon. One simple example of a vibrating body is that of a cantilever in which mass of the object is related to its frequency of vibration.

Fig. 11.1 An ordinary
cantilever

Table 11.1 The values of C_n for different harmonics

Mode of clamping	Values of C_n for different harmonics				
	C_1	C_2	C_3	C_4	C_5
Simply supported on its ends	1.6	6.28	14.1	25.1	39.3
One end free other end clamped	0.56	3.57	9.82	19.2	31.8
Both ends free, clamped at the centre	3.58	9.82	19.2	31.8	47.5
Both end clamped	3.58	9.82	19.2	31.8	47.5
One end clamped and other is hinged	2.45	7.96	16.6	20.4	43.3

11.2.1   Characterisation of Cantilever

Let us consider this phenomenon for the detection of very small mass differences
(Fig. 11.1).

A cantilever (CL) with an effective mass m^* vibrates with its fundamental
frequency f given by

$$f = (1/2\pi)(\sqrt{K/m^*}). \tag{11.1}$$

Here K is the spring constant of the cantilever and m^* is the effective mass of CL.

The ratio of effective mass m^* to the actual mass of CL is a constant, which
depends only on the geometric shape of the CL. For rectangular section, this
constant is 0.24, while for triangular sections it may be in between 0.14 and 0.18.

Equation (11.1) in a general form may be written as

$$f = C_n(1/2\pi)(\sqrt{K/m}). \tag{11.2}$$

Here C_n assumes different values depending upon the methods of clamping of the
vibrating cantilever, its geometric shape and also on the harmonics produced. The
values of C_n are given in Table 11.1 [1] for general information.

From (11.1) we see that

- For two vibrating cantilever with same spring constant, their frequency ratio is
  the square root of inverse ratio of their masses. That if f_1 and f_2 and m_1 and m_2
  are the respective frequency and mass, of the two springs, then

$$(f_2/f_1)^2 = m_1/m_2 \tag{11.3}$$

- Similarly for the vibrators having same masses their frequency ratio is equal to
  the ratio of their spring constants. That is

$$(f_2/f_1)^2 = K_2/K_1 \tag{11.4}$$

The spring constant K for a rectangular plate of length L, breadth b and thickness t is given by

$$K = Ebt^3/L^3, \tag{11.5}$$

Here E is the Young's Modulus of Elasticity.

Substituting in (11.1) frequency f for a rectangular CL is given by

$$f = \frac{1}{2\pi} \cdot \sqrt{\frac{Ebt^3}{L^3(0.24\,btL\rho)}}, \tag{11.6}$$

where ρ is the density of the material of the CL.

$$f = (t/1.96\pi L^2)\sqrt{(E/\rho)} \tag{11.7}$$

- For a given value of (E/ρ), the frequency of cantilever is proportional to the ratio of its thickness and square of its length, giving us

$$(f_2/f_1) = (t_2/L_2^2)/(t_1/L_1^2). \tag{11.8}$$

Further from (11.1) effective mass m^* of the cantilever is given as

$$m^* = (1/2\pi)^2 K/f^2.$$

Differentiating with respect to f, we get

$$0.24\,\delta m/\delta f = 2/(2\pi)^2 K/f^3.$$

- For cantilever of rectangular cross section

$$\delta m/\delta f = 0.211\,K/f^3. \tag{11.9}$$

Taking log of (11.1), we get

$$\log(f) = \log(2\pi) + 0.5\,\log(K) - 0.5\,\log(m).$$

Taking K as constant and differentiating it we get

$$\Delta f/f = -0.5\Delta m/m, \tag{11.10}$$

$$m = 0.5\Delta m(f/\Delta f).$$

Assuming that we can detect a frequency difference of one in a million, i.e. $f/\Delta f = 10^6$ in the above equation, we may calculate mass of the CL for various detectable mass differences.

11.2.2   Dimensions and Mass of an Attogram Cantilever

For example to detect a mass difference $\Delta m = 10^{-18}$ g,
   then (11.9) gives

$$m = 5 \times 10^{-13} \text{ g.} \tag{11.11}$$

Volume of a single cantilever made of silicon of density 2.5 g/cm^3 is given roughly as

$$V = 2 \times 10^{-13} \text{ cm}^3.$$

If the cantilever is in the form of rectangular plate of dimensions in the ratio of 100:10:1 with k cm as its thickness, then

$$1,000\, k^3 = 2 \times 10^{-13},$$

$$k^3 = 2 \times 10^{-16} \text{ or} = 200 \times 10^{-18} \text{ cm}^3,$$

$$k = (200)^{1/3} \times 10^{-6} \approx 6 \times 10^{-6} \text{ cm} = 0.060\,\mu\text{m} = 60\,\text{nm}.$$

That is the cantilever should have the dimensions 6,000, 600 and 60 nm.
   We may also get the idea of the mass of a cantilever by considering the frequency and spring constant of the cantilever. To achieve a resolution $\Delta f/f = 10^{-6}$, the frequency f should be of the order of a few MHz. Further to get detectable amplitude of vibration, the spring constant must be small say of the order of 0.1 N/m. Equation (11.1) then gives

$$m = K/(2\pi f)^2$$

$$0.1/39.5.10^{12}$$

$$= 0.00253 \times 10^{-12} \text{ kg} \tag{11.12}$$

$$= 2.5 \times 10^{-15} \text{ kg}$$

$$= 2.5 \times 10^{-12} \text{ g.}$$

Mass of the cantilever is 2.5 pg.

A cantilever of such dimensions is truly microscopic in nature. In order to realise such a cantilever, we need the help of nanotechnology.

11.3   Nanotechnology

Nanotechnology is one single field in which largest amount of money has been invested by both the public and private sectors. It is therefore prudent to talk about it. Before we start for its definition, let us visualise how much is a nanometre. Very roughly speaking it is one 10,000th part of the diameter of human air. Interestingly, it is roughly equal to ratio of the quadrant of earth's meridian to 1 km. However, width of the human air is quite variable and lies in between 10 and 100 μm. So a better way of visualising it will be as the length occupied by five atoms of silicon or ten atoms of hydrogen placed side by side along the straight line. Here I wish to communicate the fact that nanotechnology is dealing with the smallest parts of the matter that we can manipulate (Fig. 11.2).

Coming to its definition, one very common concept is that it is the science of measurement measuring up to or in terms of nanometre. This concept does not satisfy the vastness of the subject. Nanotechnology is rather a fundamental understanding of how nature works at the atomic scale. One important aspect of nano-industry is to convert macroscale devices such as transistors, cantilevers or electro-mechanical devices in the form of nano-scale devices. Indeed, the industry has provided us the micro-cantilever of dimensions and mass as discussed above.

Nanotechnology is driving researchers to bridge the gaps between physics, chemistry and biology. Anticipated application areas are within healthcare, environmental monitoring and life sciences. Nanotechnology can be utilised in developing portable biosensor systems, having new functions achieving high sensitivity detection of low-energy consumption and low analytic usage.

To avoid distraction of the reader from the main point, namely the detection of small mass difference with the help of micro-cantilevers, the fabrication of the micro-cantilevers is not included here. But techniques used for fabrication along with references [2–61] have been given under the heading of references. Some examples of fabrication of micro-cantilever are given.
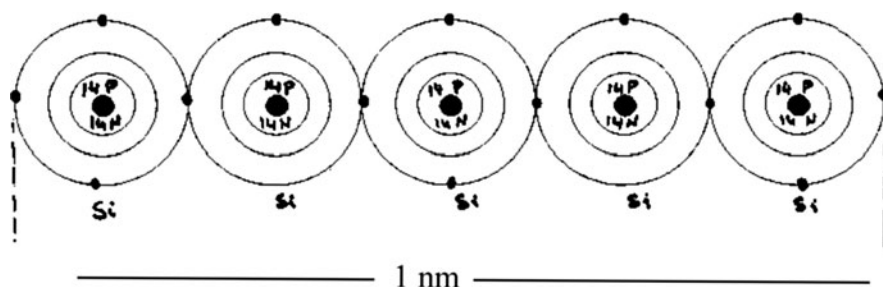

Fig. 11.2   Five silicon atoms in a straight line make a nanometre

11.4   Examples of Fabrication of Micro-cantilevers

11.4.1   Etching Process

Commercially available [62] silicon on insulator (SOI) wafers and separation by implanted oxygen (SIMOX) wafers are used as the base substrate. A fabrication technique developed for making quantum dots may be adopted for making tetrahedron silicon tips. The fabrication steps are as follows:

The tips are formed on the upper silicon layer by anisotropic etching by KOH. Local oxidation and masking by low-pressure chemical vapour deposition silicon nitride films are used to etch the desired ⟨111⟩ and ⟨100⟩ planes. Applications of the fabrication technique can be found in [63–66]. When tips are formed, a thin layer of silicon of about 100 nm thick is left unetched. This silicon layer serves as the cantilever after the sacrificial silicon dioxide layer is removed by buffered hydrogen fluoride. Fine control of the thickness is accomplished by thermal oxidation and removal of the oxide layer by buffered hydrogen fluoride. Cantilevers as thin as 30 nm are obtained by the thinning method. The length of the cantilevers is defined by the immersion time of the chip in BHF, when the sacrificial silicon oxide layer is etched. The gaps between the cantilevers and substrate are chosen by selecting the thickness of the silicon oxide layer. One aspect, which needs care, is the shape of the support of the cantilevers. The support retained the V-shaped profile of the cantilevers possibly resulting in higher support loss and multiple vibration modes. Steps are shown in Fig. 11.3.

Kawakatsu et al. [62] produced millions of cantilevers for atomic force microscopy by using the aforesaid method. The cantilevers could be tailored to measure from 500 nm to 100 μm in length and 30 to 100 nm in thickness. The
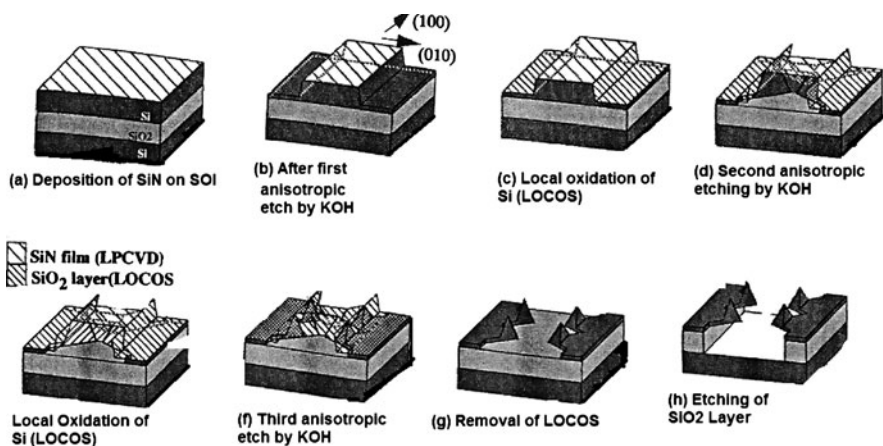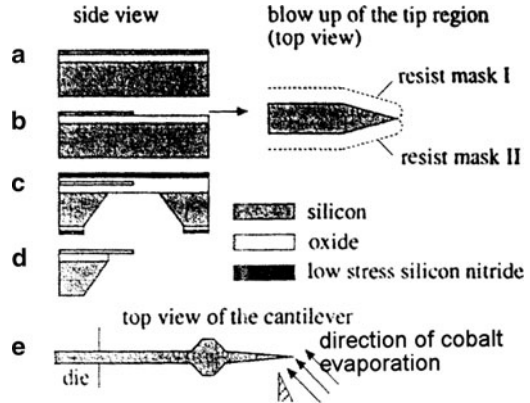

Fig. 11.3 Steps in fabrication of cantilevers

Fig. 11.4 Steps in
fabrication of cantilevers

tips and the cantilevers were formed by combination of crystal-line facets. All
cantilevers had very high degree of uniformity, well-defined shape and size. Over
1 million cantilevers per cm^2 were produced by this method. Typical mechanical
characteristics of cantilevers measuring only a few microns in length were

- Typical dimensions of cantilevers thickness 30 nm, width 500 nm and length
  100 μm.
- Spring constants a few N/m.
- Natural frequency around 10 MHz.
- Q-factor is 5 in air and 10^4 in vacuum.
- The natural frequency within a same row differed by 0.01%.
- Displacement measurement of the cantilevers from the back surface of the silicon
  substrate by infrared Fizeau's interferometer had a visibility of 0.1.

Stowe et al. [67] used the similar technique of etching in fabricating cantilever
capable of detecting forces of the order of attonewton. The cantilever processing
Fig. 11.4a starts with ⟨100⟩-oriented silicon on insulator (SOI) wafers with a top
silicon layer of 180 nm. The top thickness is reduced to desired thickness by
oxidising the surface to a required depth.

   This oxide layer is removed by using standard buffer oxide etch. Next the
cantilever and the tip are formed using two-step mask and etch process (Fig. 11.4b).
The first photo-resist mask defines the cantilever outline with a tip rounded to
0.5 μm, the limit of optical lithography. This cantilever pattern is etched into the
silicon using SF_6 plasma etches. This mask is stripped and a second photo-resist
mask containing the same pattern is applied again, but shifted to the right of the
first pattern by 1 μm. A tip forms at the intersection of the right sidewall formed
during the first etch, yielding a tip radius below 50 nm. Once the cantilevers have
been patterned, a 750 nm thick layer of low-temperature oxide and a 1.0 μm thick
layer of low stress, nitrides are deposited for topside protection. Openings in the
backside LTO and nitride are patterned and the exposed silicon is etched anisotropic
ally in 20% tetra-methyl ammonium hydroxide (TMAH). After the backside etch is

complete (Fig. 11.4c), the top nitride layer is removed using SF5 plasma etch and oxide membrane encapsulating the cantilevers is removed using BOE. The wafer is transferred under liquid from BOE to water and then from water to methanol followed by a critical point dying in high-pressure liquid CO_2. This dying step avoids meniscus forces, which can easily break or permanently curl cantilevers. Finally, silicon dyes defined during backside etch are cleaved (Fig. 11.4d). Each dye contains cantilevers that are 4–6 μm wide, 20–400 μm long. Yields over 80% have been achieved for cantilever arrays as thin as 50 nm. Figure 11.4e shows a finished 220 μm long, 60 nm thick cantilever. The cantilever design includes a 20 μm wide paddle for easy alignment of a fibre-optic interferometer to the cantilever.

11.4.2   Electron Beam Lithography

The nano-resonators are fabricated [68] from about 600 nm thick poly-silicon layer of a twin 2 poly-silicon 2-metal CMOS chip using a combination of low-energy electron beam lithography (EBL) and direct write laser lithography (DWL). The combination of low-energy EBL (3 kV) with DWL is used in order to circumvent irradiation damage of the CMOS circuitry.

After the fabrication of the CMOS, local openings are created in the top passive layer, exposing the top poly-silicon layer (Fig. 11.5(1)). The top poly-silicon layer is etched away and the bottom poly-silicon layer, which is to be used as the structural layer, is exposed (Fig. 11.5(2)). The CMOS chip is coated with a resist by layer, consisting of PMMA 950 K 1:1 on ZEP 520 A7, followed by EBL exposure (Fig. 11.5(3)). Next DWL is conducted in order to connect EBL exposed area to CMOS circuitry at the edges of the fabrication area. The structures are developed in MIBK:IPA and O-xylene (Fig. 11.5(4)), resulting in an undercut profile, which is suitable for lift-off process. Due to the irradiation damage EBL alone cannot be used since a high-energy electron beam or prolonged dwell time would be needed to fully expose the thick resist layer at the edges of the fabrication areas. After the development 30 nm of aluminium is deposited (Fig. 11.5(5)). After lift-off (Fig. 11.5(6)) the aluminium layer is used as an etch mask for the anisotropic
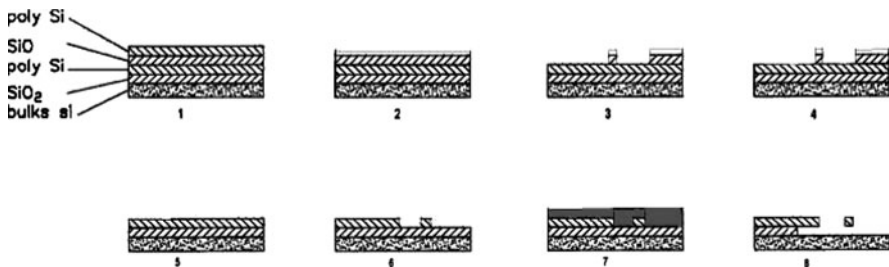

Fig. 11.5   Steps in fabrication of cantilevers

reactive ion etching of silicon, which transfers the pattern to the structural poly-silicon layer (Fig. 11.5(7)). The cantilever structure is released by HF etching of the underlying silicon oxide layer followed by extensive rinsing. Then a supportive photo-resist coating is applied to circumvent sticking of the fabricated structures. The cantilever structure is finally dry-released by removing the supportive photo-resist using oxygen plasma aching (Fig. 11.5(8)).

Nano-resonator systems have been fully integrated on a pre-processed complementary chip (CMOS). The systems have been used for high sensitivity mass sensing in air and vacuum. The resonator system, which consists of a cantilever and structure for electrostatic actuation and capacity readout, has been defined by low-energy electron beam lithography combined with direct write laser lithography on radiation-sensitive CMOS layer. The fabrication of the nano-resonator system has been conducted as a post-process step. CMOS integration radically decreases the parasitic capacitance, enabling detection of and multiplication of the resonance signal directly on the chip. Fabricated resonators systems have been designed to have resonance frequency range of 1–1.6 MHz. A mass resolution of 3 ag per Hz has been determined in air by placing a single glycerine drop at the apex of the cantilever and measuring the shift of frequency. The measured frequency shift of 14.8 kHz corresponds to added mass of 50 fg, which is close to the estimated weight of 41 fg for the glycerine drop. Mass of the drop was estimated taking into account that a glycerine drop was of 500 nm in diameter and was semi-spherical in shape with density 1.26 g/cm^3.

11.4.3   Various Micro-cantilevers in Use

Micro-cantilevers of dimensions 100–200 μm long 20–40 μm wide and 0.6 μm in thickness are commercially available from Digital Instruments, CA, and Park Scientific, CA.

Cantilevers used by various research groups in recent times are indicated in Table 11.2. The number given in the square bracket indicates the serial number of the reference. The values M, K and f are calculated from the aforesaid equations.

11.5   Principles of Detection of Micro-cantilever Motion

In practice, every micro-cantilever sensing system measures either the deflection of the beam (CL) or change in its resonance frequency. The techniques are detection of change in voltage with time, frequency, piezo-resistance or charge [73,74]; capacity of a parallel plate condenser [75,76]; use of scanning tunnelling microscope [77–79], optical lever [80] and interferometer [81,82]; and diffraction grating [83,84] to detect the change in position of the cantilever.

Table 11.2 Dimensions, shape and mass of various cantilevers

References	$L(\mu m)$	$B(\mu m)$	$T(\mu m)$	Shape	M (pg)	K	f
[69]	100	20	0.6	V	1,396	0.26 N/m	63.8 kHz
[69]	200	20	0.6	V	2,796	0.033 N/m	15.9 kHz
[69]	100	40	0.6	V	2,796	0.524 N/m	63.8 kHz
[69]	200	40	0.6	V	5,592	0.066 N/m	15.9 kHz
[70]	6	2	0.05	V	0.698	0.070 N/m	1.4 MHz
[70]	6	2	0.1	V	1.398	0.562 N/m	2.95 MHz
[86]	180	25	1	V	5,242	0.26 μN/m	32.8 kHz
[71]	350	20	0.05	V	407.8	3.5 μN/m	0.43 kHz
[62]	100	0.5	0.03	V	1,748	0.82 μm/m	3.2 kHz
[62]	100	0.5	0.1	V	5,825	30.3 μm/m	10.6 kHz
[67]	1.3	0.8	0.2	V	0.242	176 N/m	125.8 MHz
[72]	260	3.9	0.29	V	342.5	328 N/m	4.56 kHz

11.6 Examples of Detection Micro-cantilever Response

In general, there appear to be two methods of measuring the change in frequency of a cantilever. The most frequent techniques for detecting cantilever resonance are based on interferometry. Resonators can be actuated by piezo-electric, magnetic, thermal actuation or electrostatic actuation.

11.6.1 Detection by Using an Interferometer

An optical interferometer [70] with a network analyser HP4195 A and 4 mW He–Ne laser as source with normal cantilever expander, 50% cube beam splitter and 50× microscope objective is used to obtain interferogram (Fig. 11.6). A high-speed avalanche photo diode having trans-impedance amplifier is used as detector along with HP4195A as network analyser. A 4 mW modulated diode laser with wavelength 670 nm is used to excite the cantilever. The noise due to thermal excitation, i.e. continuous exchange between thermal and mechanical energy, imposes an absolute theoretical limit on the frequency stability and in turn on resolution of mass detection.

The advantage of this method is an inherent simplicity and high sensitivity; its disadvantage is related to problems of alignment, capability and portability.

11.6.2 Detection by Capacity Measurement

In this method [68], the change in capacity is measured of a capacitor formed by one fixed electrode and vibrating cantilever as the other electrode. It is achieved
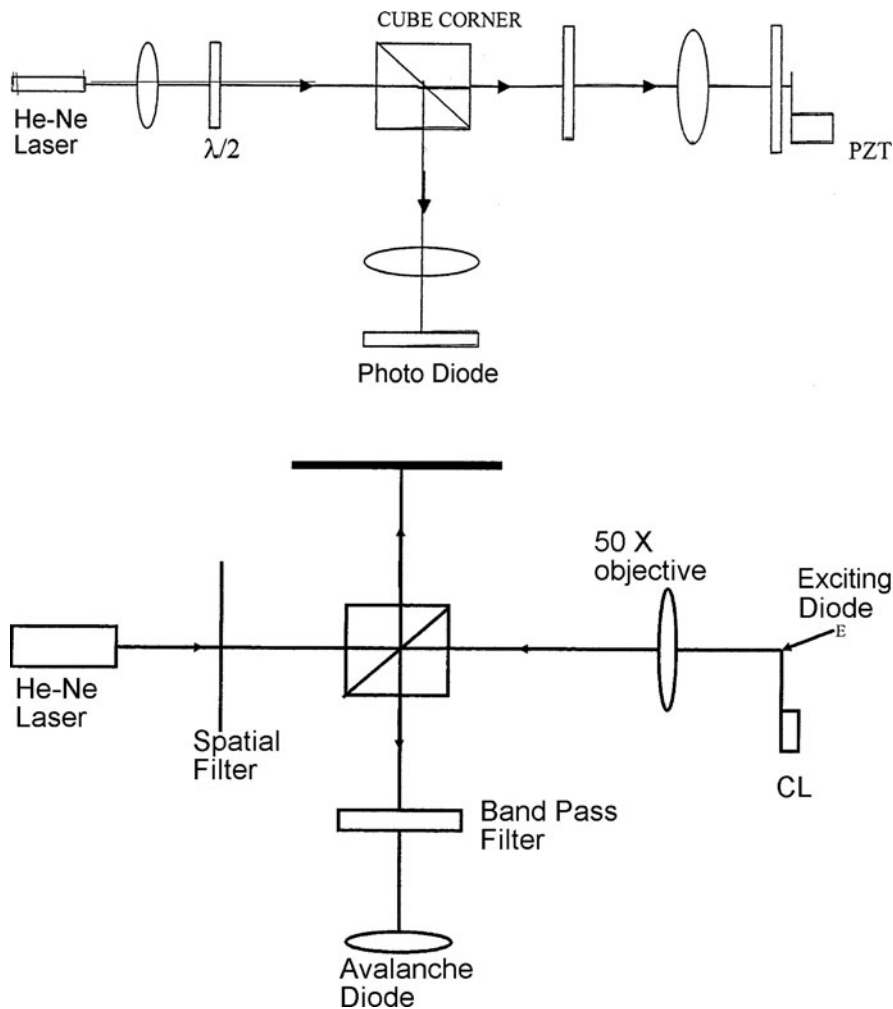
Fig. 11.6   Optical interferometer

by connecting the cantilever with standard microelectronics. The sensing principle is based on monitoring the resonance frequency of a cantilever as a function of mass adsorption, e.g. due to molecular adsorption. The nano-structure is excited into the lateral vibration by applying an AC and DC voltage between the suspended cantilever and a parallel electrode as shown in Fig. 11.7. By applying AC and DC voltage between the cantilever and a parallel fixed electrode, the cantilever is excited in a mechanical resonance. The capacitance change induces a small current, which is amplified and transformed into measurable voltage signal by the CMOS circuitry. The frequency shift upon added mass is measured on a chip by capacitive resonance frequency detection. Sensitivity of the cantilever is three attogram per Hz.
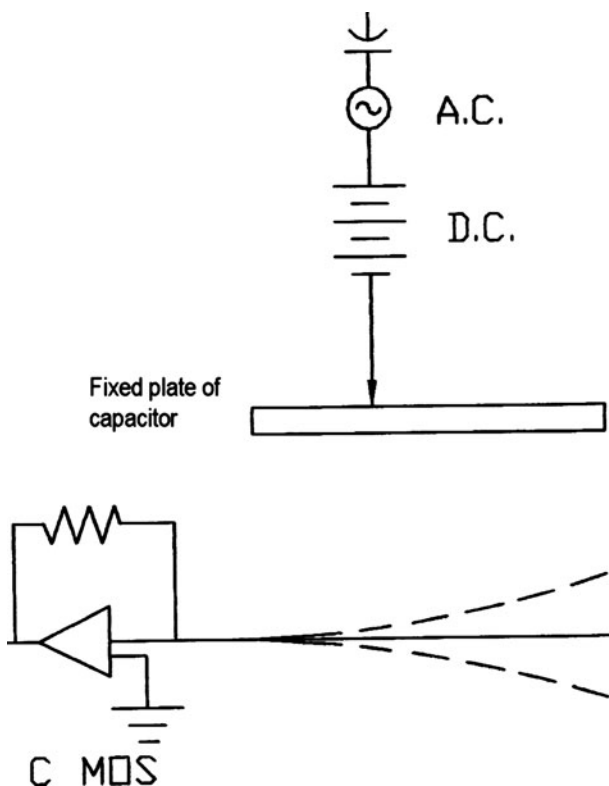
Fig. 11.7 Capacitance detection

As the CL vibrates close to the parallel electrode the capacitance change induces a displacement current given by

$$I = C\delta V/\delta t + V\delta C/\delta t.$$

The first term is the current contribution from the static capacitance and second term is current contribution from the mechanical oscillation of the cantilever. The current is amplified and converted into a measurable voltage signal by an integrated electronics on the CMOS chip. CMOS integration reduces parasitic capacitance contribution and is hence crucial for the choice of a cantilever readout. Furthermore CMOS allows for increased functionality in terms of frequency tracking and Q-factor enhancement.

A nanometer system can be used for label-free detection of molecules or particles with high spatial control. CMOS integration results in a small and compact system with simple operation, which could be used as a component in a portable device. The resonator systems are integrated on a $15.15\,\text{mm}^2$ CMOS chip. On each CMOS chip, up to 50 resonator systems are fabricated, which also allows for parallel mass detection.

11.6.3   *Improved Fibre-Optic Interferometer*

The schematic diagram of the interferometer is shown in Fig. 11.8. A multi-mode Gallium Aluminium Arsenide (GaAlAs) diode ($\lambda = 830$ nm) with a direct single-mode fibre output is used as a light source. The light is coupled to the input (labelled 1) of a 2×2 single-mode directional coupler. The coupler splits the incident beam equally between leads 2 and 3, which carry the light to the cantilever and the reference photodiode respectively. Approximately 4% of light in lead 2 is reflected from the glass–air interface at cleaved end of the fibre. This reflected light comprises one of the two interfering beams. The other 96% light exits the fibre and impinges on the cantilever with spot size of the order of a few micrometres. Part of this light is scattered back into the fibre and interferes with the light reflected from the fibre end. The total optical power reflected back through the fibre depends on the phase difference between the fibre end reflection and the cantilever reflection. The coupler directs the half of the total reflected light to lead 4 and into the signal photodiode, where the intensity of the optical interference pattern is measured. To reduce reflections from the ends 3 and 4 the fibre ends were cleaved at a non-orthogonal angle and index-matching liquid was placed between the photodiode and the fibre ends.

   The output of the signal photodiode can be used directly as the signal. However, better performance is obtained especially at frequencies below 1 kHz, if laser amplitude noise is cancelled by either subtracting or dividing the output signal by the output signal from the reference photodiode. Since most of the divider circuits have somewhat limited dynamic range, it is better to chose noise subtraction approach using a low-noise differential amplifier.
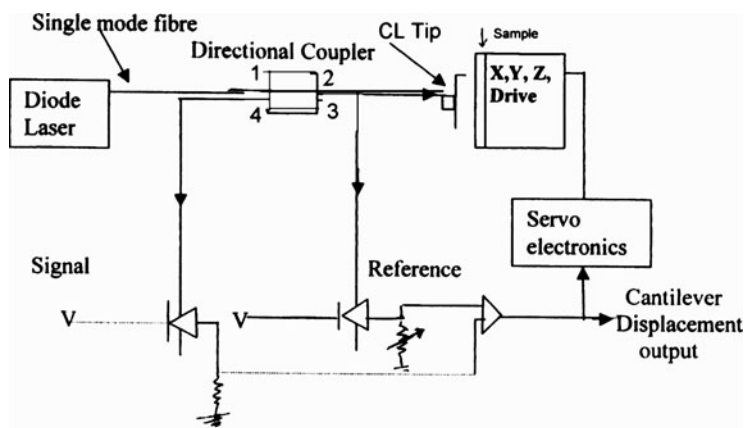

Fig. 11.8 Fibre-optical interferometer

11.7 Mass Sensitivity of Cantilevers

Mass sensitivity of a cantilever is defined [69] as the relative change in frequency for change in mass per unit area. Normally area is taken in cm^2. Symbolically S_m the mass sensitivity of the cantilever is

$$S_m = \lim(\Delta f / f)(1/\Delta m) = (d f/dm)/f. \tag{11.13}$$

Here Δm or dm is the change in mass per unit active surface area of the cantilever. That is Δm = change in mass/effective area of the cantilever.

The frequency changes due to two reasons, namely (1) change in the spring constant and (2) change in mass deposited on unit area of the cantilever. Two cases arise.

Case 1: Mass is deposited on the cantilever in such a way that there is no change in spring constant, i.e. end-point loading.
Case 2: Mass deposition is uniform on the certain effective area of the cantilever affecting the change in spring constant also.

11.7.1 No Change in Spring Constant (End-Point Loading)

Let a mass m be added to the cantilever system, such that spring constant remains unchanged, i.e. t remains unchanged; the frequency f from (11.6) is given by

$$f = \{Ebt^3/4L^3(m + 0.24btL\rho)/2\pi\}^{1/2}. \tag{11.14}$$

Taking log of both sides, we get

$$\log(f) = 0.5\log(Ebt^3/L^3) - 0.5\log(m + 0.24\, btL\rho) - \log(2\pi).$$

Differentiating partially with respect to m

$$\delta f/f = -\delta m/2(m + 0.24\, bLt\rho). \tag{11.15}$$

If mass m is spread over uniformly on an effective surface ξbL of the cantilever, then

$$m = \xi bLt_d\rho.$$

Here t_d is the thickness of the material. The density ρ of mass deposited is same as that of the material of the cantilever.

Substituting the value of m in (11.15), we get

$$\delta f/f = -\delta m/2(\xi bLt_d\rho + 0.24btL\rho)$$
$$= -\delta m/2bL(\xi t_d + 0.24t)\rho, \tag{11.16}$$

but change in mass per unit area $= -\delta m/\xi bL$, giving us

$$S_m = (\delta f/f)/(\delta m/\xi bL) = -\xi/(\xi t_d + 0.24t)2\rho,$$
$$S_m = -\xi/2\rho(\xi t_d + 0.24t). \tag{11.17}$$

Negative sine means that frequency will decrease if mass of the cantilever increases.

11.7.2 Changing Spring Constant (Uniform Loading)

If the mass of cantilever is varied by depositing the material uniformly over its surface area (bL) then from (11.7) f is given by

$$f = (t/1.96\pi L^2)\sqrt{(E/\rho)}, \text{ giving us}$$
$$\delta f/f = \delta t/t \text{ and}$$
$$\delta m = \text{change in mass} = \rho bL\delta t.$$

So change in mass per unit area $= bL\delta t\rho/bL = \rho\delta t$.

$$S_m = (\delta f/f)/\rho\delta t$$
$$= (\delta t/t)/\rho\delta t, \text{ giving}$$
$$S_m = 1/\rho t. \tag{11.18}$$

Here positive sign indicates that frequency will increase with the increase in mass of the cantilever.

In micro-cantilever literature the expression "minimum detectable mass density" is frequently abbreviated as MDMD.

Minimum detectable mass density (change in mass per unit area)

$$\text{MDMD} = \Delta m_{min} = (1/S_m)\Delta f_{min}/f. \tag{11.19}$$

Typical range of values of MDMD for micro-cantilevers is $(0.02–0.04)\,\text{ng/cm}^2$.

11.8 Mass Detector Cantilevers

11.8.1 At Femtogram Level

Lavrik and Datskos [73] at Oak Ridge National Laboratory used a rectangular gold-coated silicon cantilever with resonant frequency of 2.25 MHz and exposed it to

11-mercaptoundecanoic acid (MA) vapours. The cantilever was mounted in an open cell. Heating small amount of powdered acid to 60°C generated adequate vapour pressure. The resonance frequency of the cantilever showed a significant change on exposing it to vapours. Chemisorptions of the acid molecules took place only on to the gold-coated surface of the cantilever. Change in mass of the resonating cantilever was estimated from the formula:

$$\Delta M = G \ K / \pi^2 (1/f_1^2 - 1/f_o^2) \cong 2G \ K \Delta f / f o^3. \tag{11.20}$$

Here G is a geometrical factor of the cantilever (1.37) and Δf is the change in frequency. The smallest frequency shift, which they measured, was of 2 kHz; in a micro-cantilever with $K = 0.1$ N/m and resonant frequency of 2.2 MHz, the mass of the acid added to the cantilever was

$$\Delta M = 2 \times 1.37 \times 2.10^3 \times 0.1/(2.2 \times 10^6)^3 = 0.051 \times 10^{-15} \text{ kg} = 5.1 \text{ fg}.$$

This value is very close to the mass of a single molecular layer of the acid covering only 50% of gold-coated area of the cantilever.

11.8.2 At Attogram Level

Craighead and co-workers at Cornell University US have optimised the cantilevers for mass detection to new level. Using their extensive experience with nanofabrication techniques and by conducting experiments with various types of electro-mechanical devices, the team has managed to improve the limit of mass detection to 10^{-18} g [85, 86].

In Fig. 11.9, a gold dot, about 50 nm (nanometres) in diameter, is fused to the end of a cantilevered oscillator about 4 μm long. A one-molecule-thick layer of a sulphur-containing chemical deposited on the gold adds a mass of about 6 ag, which is more than enough to be measured.

It may be noted that the mass of a small virus is about 10 ag. So such cantilevers are being used for detecting viruses as well.
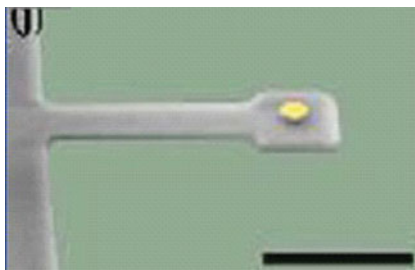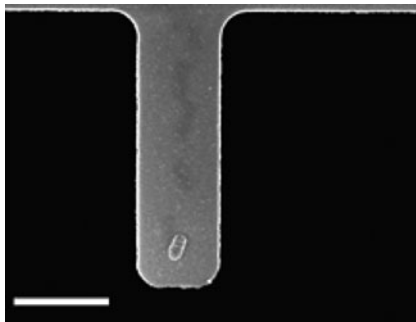

Fig. 11.9 50 nm gold spot on a micro-cantilever (Craighead Group/Cornell University)

Fig. 11.10 Courtesy
Craighead Group/Cornell
University

11.8.2.1   Single Cell Detection

For cell detection, the cantilever is coated with antibodies that bind to *E. coli* bacteria
[87]. The device is then bathed in a solution containing the cells. Some of the
cells will bind to the surface, and the additional mass will change the frequency
of vibration. In one case just one cell happened to bond to a cantilever, and it was
possible to detect the mass of the single cell.

Scanning electron microscope photo of a single cell bound to the antibody layer
on top of the oscillator is shown (Fig. 11.10). The cell is 1.43 mm long and 730 nm
wide. Its estimated mass is 665 fg (665×10^{-15} g).

11.8.3   Sub-attogram Level

A very high-quality micro-oscillator fixed at both ends having Q-factor of 20700
[88] was able to detect 0.37 attogram. The next milestone in nano-electro-
mechanical mass detection is to achieve zeptogram (10^{-21} g) sensitivity, which
will prove whether nanomechanical mass spectroscopy is feasible.

11.8.4   Zeptogram Level

Bachtold and his team of scientists in Spain [89] have developed a carbon nano-
tube of 1 nm diameter which is clamped at both ends to two electrodes (Fig. 11.11).
Mass sensitivity is 11 Hz yg^{-1} At room temperature, the nano-tube resonator has a
resolution of 25 zg, but cooling the nano-tube down to 5 K the resolution improves
to 1.4 zg. The team of Bachtold is improving the measurement set-up and hoping to
achieve in the near future the resolution of 0.001 zg.

Roukes et al. at California Institute of Technology [90] have also developed very
high-frequency (VHF) nano-electro-mechanical systems (NEMS) which provide a

Fig. 11.11 Micro-cantilever

300 nm
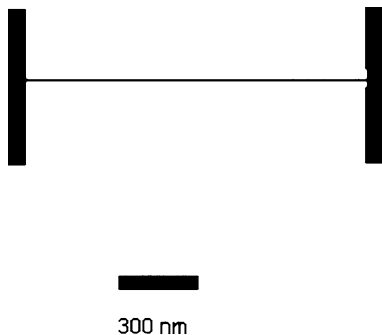
very high sensitivity for inertial mass sensing. The group has demonstrated in situ measurements in real time with mass noise floor $\sim$20 zg. Their best mass resolution corresponds to $\sim$7 zg, equivalent to $\sim$30 xenon atoms or the mass of an individual 4 kDa molecule. Detailed analysis of the ultimate sensitivity of such devices based on these experimental results indicates that NEMS can ultimately provide inertial mass sensing of individual intact, electrically neutral macromolecules with single-Dalton (1 amu) resolution.

11.8.5 Sub-zeptogram Level (One Gold Atom)

A double-walled nano-tube, which consists of two concentric rolled-up sheets, is anchored to an electrode at one end. When an object is placed on a device, another electrode at the free end causes the nano-tube to oscillate at a frequency proportional to the mass of the object. The device has a sensitivity of 1.3×10^{-22} gHz$^{-1/2}$. Mass of a single atom of gold has been detected with the device [91]. As nano-tubes are smaller than the wavelength of light, standard optical techniques for detecting vibrations fail. The vibrations, therefore, are detected electronically. A line diagram is shown in Fig. 11.12. Figure 11.12a depicts the nano-tube, Fig. 11.12b illustrates ultrahigh vacuum chamber and method of production and sending the gold atoms to the nano-tube device and Fig. 11.12c the electronic circuit.

Some very good papers on detection at zeptogram level have been published by Roukes and Ekinci group [92–94].

11.8.6 At Attonewton Level

Stowe, Yasumura and Kenny [67] at Stanford University used a 60 nm thick cantilever at 4.8 mK to obtain a resolution of $(5.6 \times 10^{-18}\,\text{N})/\sqrt{\text{Hz}}$.

Mamin and Rugar [95] at IBM, in 2001, used cantilever to detect a sub-attonewton force using infrared laser of 1.5 μm to detect the change in frequency.
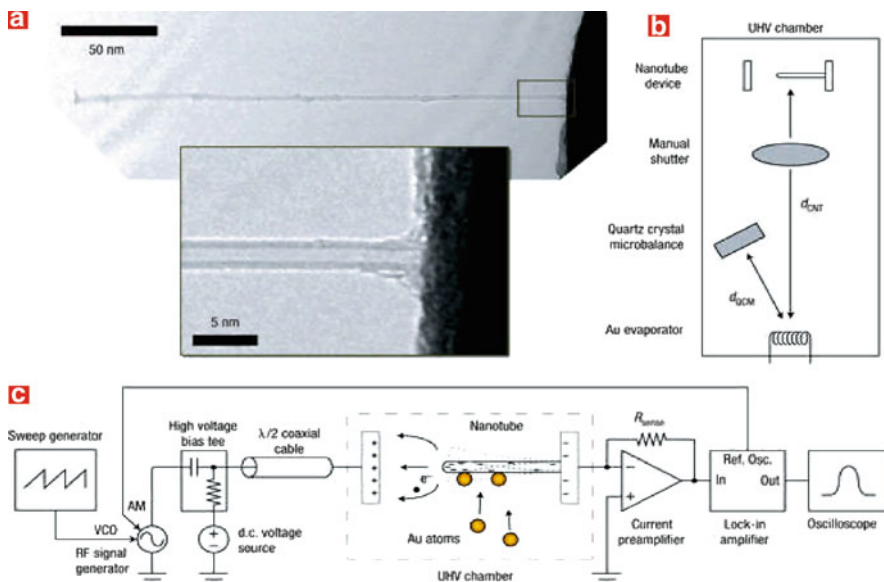
Fig. 11.12 Concentric carbon nano-tube, ultrahigh vacuum chamber and electronic circuitory. "Courtesy Zettl Research Group, Lawrence Berkeley National Laboratory and University of California at Berkeley"

The cantilever was cooled down to $110\,\mathrm{mK}$ to reduce its thermal noise to $10^{-21}\,\mathrm{N}$ in a 1 Hz bandwidth.

11.8.7   A Final Goal

One of the challenges of nanotechnology and nanomechanics is having a mass spectrometer working at subatomic level. The maximum resolution had been achieved with some silicon resonators (with a resolution of about 1.4 zeptograms at a temperature of 4.2 K). Now, the work of Bachtold and co-workers has substantially increased that resolution through the use of carbon nano-tubes.

The mass of a nano-tube is very low, barely a few attograms so that any tiny amount of added mass will be detected. In addition, the nano-tubes are mechanically ultra rigid, which makes them excellent candidates to be used as mechanical resonators.

Now, team of Bachtold is improving the measurement set-up and hopes to achieve in the near future the resolution of 0.001 zg, the mass of one nucleus. The researchers will then place proteins on the nano-tube and monitor the change of the mass during chemical reactions (when a hydrogen atom is released from the protein, for instance).

Nanotechnology has been advancing rapidly in the few last years. Even so, there remain many challenges ahead, and one of them is a mass spectrometer to allow work at that level, with small biological molecules or atoms.

The development Bachtold team has coincided in time with others of similar characteristics, both from the USA. One is at the Technical University of California (Caltech) and the other is at the University of California (Berkeley). Both groups have developed mass sensors based on carbon nano-tubes, with minor differences between the methods used.

11.8.8   Viscosity: A Problem

Nanomechanical resonators enable the measurement of mass with extraordinary sensitivity. Previously, samples as light as 7 zg have been weighed in vacuum, and proton-level resolution seems to be within reach. Resolving small mass changes requires the resonator to be light and to ring at a very pure tone—that is, with a high-quality factor. In solution, viscosity severely degrades both [96]. Thus preventing many applications in nanotechnology and the life sciences where fluid is required. Although the resonant structure can be designed to minimise viscous loss, resolution is still substantially degraded when compared to measurements made in air or vacuum. An entirely different approach eliminates viscous damping by placing the solution inside a hollow resonator that is surrounded by vacuum. The group has demonstrated that suspended microchannel resonators can weigh single nanoparticles, single bacterial cells and sub-monolayers of adsorbed proteins in water with sub-femtogram resolution (1 Hz bandwidth). Central to these results is the observation that viscous loss due to the fluid is negligible compared to the intrinsic damping of our silicon crystal resonator. The combination of the low resonator mass (100 ng) and high-quality factor (15,000) enables an improvement in mass resolution of six orders of magnitude over a high-end commercial quartz crystal microbalance. This gives access to intriguing applications, such as mass-based flow cytometry, the direct detection of pathogens or the non-optical sizing and mass density measurement of colloidal particles.

11.9   Minimum Detectable Force/Mass

The noise due to thermal excitation, i.e. continuous exchange between thermal and mechanical, imposes an absolute theoretical limit on the frequency stability and in turn, threshold mass sensitivity of any nanomechanical resonator [67]. By equating mechanical energy to thermal energy of the vibrating cantilever, we get

$$m\omega^2 z_o^2/2 = k_{\mathrm{B}}T, \tag{11.21}$$

where k_{B} is the Boltzman constant and T is the absolute temperature in K.

We can calculate minimum detectable mass ΔM_{min} and minimum detectable force ΔF_{min}. The values of minimum detection mass or force can be expressed in several ways by taking combinations of mass and dimensions of the cantilever; one such set of expression is given as

$$\Delta F_{min} = \sqrt{(K k_B T / 2\pi f_o Q z^2)}. \tag{11.22}$$

In terms of mass and spring constant of the cantilever, the minimum detectable mass ΔM_{min} is given as

$$\Delta M_{min} = (8 G m_o^{5/4} [k_B T \Delta f] / \{(z^2)^{1/2} K^{3/4} \sqrt{Q}\})^{1/2},$$
$$\Delta f_{min} = (bt^2 / LQ)^{1/2} (E\rho)^{1/4} (k_B T B)^{1/2}. \tag{11.23}$$

11.10   Micro-cantilever Applications

The methods of fabrication and determination of micro-cantilever deflection or frequency change have been discussed. Cantilevers have large surface to volume ratio and hence can be used to detect adsorbed gasses or other elements on surfaces of the artefacts. Other applications of micro- and nano-cantilevers are also being discussed.

11.10.1   Large Surface to Volume Ratio

We see from above that all cantilevers have much smaller thickness in comparison to other dimensions, giving a very large surface to volume ratio.

Taking the cantilever of rectangular cross section for simplicity, surface of a cantilever is $2(Lb + bt + tL)$ and volume is given as Lbt

$$\text{Ratio of surface to volume} = 2(bL + bt + tL)/Lbt$$
$$= 2(1/t + 1/L + 1/b).$$

Normally t is of the order of $100\,\text{nm} = 10^{-7}\,\text{m}$, $b = L/10$ and $L = 100\,\mu\text{m}$, giving us

$$\text{Surface/volume} = 2(10^7 + 10^4 + 10^5) \approx 2 \times 10^7.$$

Here we see that surface area is very large relative to its volume. From above discussions, it has become amply clear that any surface phenomenon can be studied with the help of a micro-cantilever.

11.10.2   Examination of Surface

Probably the earliest applications of micro-cantilevers were to map out surface topographies using the STM and AFM with sub-nm resolution. These are so-called contact techniques, where the probe tip was dragged over the surface, hence producing the micro-cantilever detection. This microscopy approach is not feasible for softer surfaces such as biological cells, as the micro-cantilever probe tip will damage the entity to be imaged. Therefore, tapping mode microscopy was developed, which holds the probe tip away from the surface and actuates it, often piezo-electrically and usually at the fundamental resonance frequency of the micro-cantilever, and then monitors changes in the resonance frequency that occur due to the van der Walls-type attraction that occur as the probe tip is brought closer to the entity being imaged or by actual tip-entity contact. The tapping mode has been successfully demonstrated in both air and liquid environments [97]. Lateral force microscopy is similar to the contact mode AFM approach except that the motion of the beam is now in the direction of the beam width, so that tip–surface interactions can cause the micro-cantilever to detect in the thickness direction and to exhibit torsional deformation, which can be monitored and used to map out surface topography; an example is given in reference [98].

The flexibility to choose between contact mode, tapping mode and near-field mode allows micro-cantilever microscopy to be applied to a wide range of materials. Multiplexed microscopy is feasible in a rapid, automated and parallel fashion using multi-cantilever arrays [99].

11.10.3   Thermal/Photo-thermal

The micro-cantilever has proven useful in thermal and photo-thermal imaging as well. Infrared detection systems, in which the micro-cantilever detection is a function of the light intensity incident upon the beam, have been produced [100]. The beam detection is due to either a temperature gradient through the thickness of the beam or a bimetallic effect if the micro-cantilever is composite in nature (the beam materials need not be metallic though). The bimetallic effect has also been used to detect enthalpy-induced temperature shifts (i.e. phase changes) and to obtain photo-thermal heating as a function of frequency to provide absorption spectra for certain materials [101, 102].

Thundat et al. [69] used nano-cantilevers having a metallic coating on one side. The coating with silicon gives the bimetallic effect. Due to very small change in temperature, the cantilever bends and its bending is measured. The cantilever demonstrated the ability to detect power as small as 100 pW and energy 150 fJ. The limit of temperature detection was 10^{-5} K. The bending of the lever is proportional to the heat energy absorbed in the cantilever. The maximum detection $z_{\max}$ due to differential stress is given by [103]

$$Z_{max} = \{5(t_1 + t_2)t^3/4(\lambda_1 t_1 + \lambda_2 t_2)bt_2^2\}x$$
$$[\{(a_1 - a_2)dQ/dt\}/\{4(L + t_1^2/t_2^2) + (1/t_1 t_2)(6t_1^2 + E_1 t_2^2/E_2) + E_1 t_1^3/E_2 t_2^3\}],$$

where dQ/dt is the rate of incident energy, L and b are the length and breadth of the cantilever, t_1 and t_2 are the thickness of the two layers and λ_1 and λ_2, α_1 and α_2 and E_1 and E_2 are the thermal conductivities, thermal expansions and Young's modulus of elasticity of the two layers, respectively.

11.10.4   Low Power Consumption Micro-cantilevers

The portability, compactness, price and deployment of sensing systems are determined largely by power consumption and simplicity of the sensing platform. Adam et al. [104] fabricated a micro-cantilever system for chemical detection. It was based on an array of piezo-electric micro-cantilevers. The power consumption of sensing element array including actuation was measured in nano-watts, with impedance of the order of megaohms. This was four to five orders of magnitude lower dissipation than the contemporary cantilever chemical detection platforms using optical or piezo-resistive detection. The sensor was in picowatt region. The platform consisted of three cantilevers wires in series, where variation of resonant frequency and quality factor of selectively coated cantilevers, during successive impedance measurements, enabled the detection of ether vapours.

11.10.5   Chemistry

The micro-cantilever as applied to the chemistry and biology fields involves the sensing of bonding or conformational change events that occur on one (or both) side of a micro-cantilever. Bonding events on both sides will increase the mass and hence change the resonance frequencies of a micro-cantilever but, assuming equal bonding on both sides, will not cause a static deflection. The term bonding is broad and does not necessarily refer to a bona fide chemical bonding event. For example, monitoring of micro-cantilever resonance frequency when oscillating in air with increasing humidity will show the resonance frequency drop due to moisture clinging to the beam surface [105].

Cantilevers of millimetre size are available, which can detect accurately the presence of volatile organic compounds [106]. The frequency dependence on change in mass is measured to be 0.06 Hz/ng. In gas detection, the minimum detectable concentration of ethanol of 14 parts per millions has been achieved.

11.10.6   Biology

Another type of bonding involves functioning of one (or both) surface(s) of the micro-cantilever with a half of a DNA sequence followed by immersion of the micro-cantilever in a fluid solution containing the complementary DNA sequence. The surface stresses and lowered amount of conformational states available to the DNA after hybridisation will cause a beam to deflect [107]. Applications of such micro-cantilevers are remarkably sensitive, and can determine if a single *E. coli* cell has bonded to the beam [108]. Wu et al. showed that micro-cantilevers of different geometries can detect prostate-specific antigens (PSA) in concentrations from $0.2 \, \text{ng/cm}^3$ to $60 \, \mu\text{g/cm}^3$, which includes the clinically relevant range [109]. McKendry et al. performed similar experiments with DNA but used eight cantilevers, each coated with a different thiolated probe treatment to allow for multi-plexed DNA hybrid detection [110]. By judicious treatment of micro-cantilevers, these are used to sense the presence and concentration of a variety of liquid- or air-borne substances.

Micro-cantilevers are used [111] to detect DNA strands with a specific sequence using gold nanoparticle modified DNA. The shift of the cantilever frequency signals the binding events. The method can detect target DNA at a concentration of 0.05 nmol or lower. Multiple DNA detection is possible by coating multiple cantilevers with various capture DNA strands and measuring the change in resonance frequencies.

11.10.7   Health Care

According to data present by the Centre for Disease Control and Prevention USA, TB remains as one of the most challenging health problems. TB is transmitted by aerosol droplets from TB carrier and can be captured by cantilever sensors with immunoreactions. Microfabrication technologies utilised in Micro-Electro-Mechanical Systems provide a way for low-cost high-throughput production of miniaturised cantilever based on TB assays. Besides TB, other pathogens, such as anthrax, influenza, measles, chickenpox and smallpox as well as hazardous chemical pollutants in atmosphere, can all invoke immune responses and be monitored qualitatively and quantitatively with arrays of the cantilever sensors [112].

A team of Physicist, Biochemist, and Physicians has constructed an array of cantilevers of sub-millimetre size [113]. The array can measure the concentration of proteins, which gives information about the health of the person's heart. It promises the diagnoses of heart attacks quicker and easier than any existing technologies. The array consists of eight cantilevers that are each 0.5 mm long, 0.1 mm wide and 500 nm thick. The upper surface is coated with blood–protein antibodies. When the array is immersed in liquid containing blood protein, the antibodies bind protein.

This induces a stress in the cantilevers and causes them to bend and make diagnoses of heart condition possible.

A micro-scale, robust, real-time monitoring micro-machined ultra-thin cantilever arrays are being developed at the Perdue University, West Lafayette, Indiana. These are meant for the sensitive detection of infectious and bioterrorism agents in field setting and in primary-patient care facilities. The array will be specific for pathogens and will have the sensitivity to detect single virus or toxin molecule. During phase I, efforts will aim to develop dielectro-phoresis-based infectious agent trapping, separation and consent proof-of-principle demonstration for the detection of air-borne virus on special micros. The performance value of the devices for trapping, separation, concentration and detection of corona-virus particles will be assessed. During phase II, this sensor design and manufacturing can be extended and scaled up to other infectious agents in the form of integrated sensor arrays with broad signalling process.

11.10.8 *Physics (Viscosity and Density)*

By immersing micro-cantilevers in tiny volume ($<1\,\text{nL}$) liquid samples and observing resonance (and resonance shift) behaviour, viscosity can be determined [114, 115]. These early efforts were only valid for liquid viscosity determination and required a priori knowledge of the liquid density. The method, therefore, was refined to apply to determination of gas viscosity as well, negating the need for a priori fluid density knowledge [116].

The resonance frequency of a cantilever is affected by damping due to surrounding medium. Mathematically according to [69] a cantilever is a one-dimensional damped harmonic oscillator with a spring constant K and effective mass m^*. Due to the viscous nature of the medium, a determinable volume of it is carried along the lever through oscillation cycle. This induced mass m_j is equivalent to the mass of the semi-sphere of radius R of the medium and is given as

$$m_j = 2\pi R^3 \rho/3. \tag{11.24}$$

R is empirically determined; therefore, the effective mass m' of the cantilever will become

$$m' = m^* + m_j.$$

For systems of large Reynold's number and excitation amplitudes that are much less than the cantilever length, the drag force F may be written as

$$F = b(\mathrm{d}y/\mathrm{d}t) + (m_j/\omega)\mathrm{d}^2 y/\mathrm{d}t^2. \tag{11.25}$$

b/m' is defined as the dissipation constant. The second term in (11.25) is due to the induced mass carried along with the lever in the medium. In the case of a sphere in

the medium, the dissipation constant is given by

$$B = b/m' = 3\pi R^2 (\sqrt{2\eta\rho\omega})/m', \tag{11.26}$$

where ρ is the density of the medium, ω is the oscillation frequency of the oscillator and η is viscosity of the medium. From this, the frequency for maximum amplitude response of the system is given as

$$\omega_{\max} = (1/8)\{\sqrt{9B^4 + 64\omega_0} - 3B^2\}. \tag{11.27}$$

ω_0 is the undamped peak resonance frequency. The geometric factor n and R should be invariant for a given cantilever for given medium and are determinable by fitting to the cantilever response data.

The Q-factor of the vibration is defined as

$$Q = \sqrt{3}\omega/B.$$

Using $\omega^2 = K/m'$ the virtual mass m' can be expressed

$$m' = 4K/\omega^2 (4 + 9/Q^2). \tag{11.28}$$

Using (11.26) and (11.27) an expression of viscosity η may be written as

$$\eta = 8K^2/[3\pi^2 R^4 n^2 \rho\omega^3 Q^2 (4 + 9/Q^2)]. \tag{11.29}$$

Our initial results show that micro-cantilever can be used for sensitive detection of viscosity of liquids. The density of the fluid can be determined from the Q-factor the cantilever resonance and other parameters as

$$\rho = (3/2\pi R^3)[4K/\omega(4 + 9/Q^2) - m^*]. \tag{11.30}$$

Method is highly useful for the liquids which are available in very small quantities say of the order of nanolitres.

11.10.9 Magnetometry

In magnetic force microscopy (MFM) a magnetic tip is mounted to, or manufactured on, a micro-cantilever, which is scanned in a non-contact fashion above a surface. Beam detection and resonance usually are obtained using piezo-electrics or optical levers. In static mode, the detection is monitored resulting in a force image, while in dynamic mode the resonance behaviour monitoring allows for a force gradient image. Rudnitsky et al. used MFM to sense the location of magnetic particles that were tethered to a substrate [117], while others have used MFM to examine the

magnetic domain structure of thin films under imposed strain and examine electron spin configurations resulting in a claimed sensitivity of two electron spins [118,119].

11.10.10 *Data Storage*

A relatively new application of tipped micro-cantilevers is in the field of data storage. The tip is scanned over a polymeric film and at desired locations it is heated (usually by subjecting it to a bias voltage), pressed in to the polymer film, and removed leaving a small pit impression in the film. In the "write" mode the cantilever makes numerous such pits at certain locations to define the zeros and ones, which define a data set [120]. In "read" mode, the pits are scanned over, basically using the cantilever as an AFM [121]. Finally, in "erase" mode, the pits are produced very close to each other, and this results in leaving behind a polymer film surface that is only mildly disturbed from the initial state, a surface undisturbed enough so that it can be "rewritten" upon [122]. More recent work has shown that this technique may be capable of storage densities one or even more orders of magnitude larger than the current technology of magnetic-based storage [123].

11.10.11 *Terrorist Threat Detection*

Recent terrorist events have envisaged the urgent and widespread need for development of novel sensors for threat environment. The advent of inexpensive, mass-produced micro-cantilever sensors, promises to bring about a revolution in detection of terrorist threats. Extremely sensitive and highly selective sensors can be developed for the detection of chemical, biological and radiation threats using micro-cantilever platform. Micro-cantilever resonance such as resonance frequency, deflection, and Q-factor undergo variation due to extremely small changes in external stimuli. Cantilever geometry determines sensitivity while selectivity is governed by analyte–substrate interaction mechanism. A large number of sensors for explosive, chemical agent, biological weapons and radiation are being developed using micro-cantilever platform. An array based approach offers the flexibility of multiple analyte detection using the single sensor platform.

References

1. A. Eugene, *Avallone and Theodre Baumister Mark's Standard Handbook for Mechanical Engineers*, 9th edn. (McGraw-Hill Book by III), pp 5–74
   Silicon Micro-machining
2. J.W. Gardner, *Microsensors: Principles and Applications* (John Wiley & Sons, 1994)
3. M. Madou, *Fundamentals of Microfabrication* (CRC Press, 1997)

4. N. Maluf, *An Introduction to Microelectromechanical Systems Engineering* (Artech House, 1999)
5. S.D. Senturia, *Microsystem Design* (Kluwer, 2000).
   Non-IC Based Micro Machining
   Silicon Micro Machining
6. P.A. McKeown, From micro to nano-machining towards the nanometer era. Sensor Rev.**16**(2), 4–10 (1996)
7. M. Nakao, Y. Hatamura, A tabletop factory to fabricate micro-machines, nano manufacturing world. Proc. ASPE **14**, 74–79 (1996)
8. N. Mishima, K. Ashida, T. Tanikawa, H. Maekawa, K. Kaneko, M. Tanaka, Micro-factory and a design evaluation method for miniature machine tools. Proc. Int. Workshop Microfactories. 155–158 (2000)
9. Y. Takeuchi, H. Yonekura, K. Sawada, Creation of 3d tiny statue by 5-axis control ultra precision machining. Computer Aided Design. **35**, 403–409 (2003)
10. T. Schaller, L. Bohn, J. Mayer, K. Schubert, Microstructure grooves with a width of less than 50 cut with ground hard metal micro end mills. Precision Eng. **23**, 229–235 (1999)
11. D.P. Adams, M.J. Vasile, G. Benavides, A.N. Campbell, Micromilling of metal alloys with focused ion beam-fabricated tools, Precision Eng. **25**, 107–113 (2001)
12. C.R. Friedrich, M.J. Vasile, Development of the micromilling process for high aspect ratio microstructures. J. Microelectromech. Sys. **5**, 33–38 (1996)
13. Y.N. Picard, D.P. Adams, M.J. Vasile, M.B. Ritchey, Focused ion beam-shaped microtools for ultra-precision machining of cylindrical components. Precision Eng. **27**, 59–69 (2003)
14. H. Weule, V. HÄuntrup, H. Tritschler, Micro-cutting of steel to meet new requirements in miniaturization. Ann. CIRP **50**, 61 (2001)
15. Z. Lu, T. Yoneyama, Micro cutting in the micro lathe turning system. Int. J. Machine Tools Manufact. **39**, 1171–1183 (1999)
16. Y. Okazaki, T. Kitahara, NC micro-lathe to machine micro-parts. Proc. ASPE **22**, 575–578 (2000)
17. A. Bohart, P. Collins, S. Faulk, C. Halvorson, M. McClellean, K. Shillito, Affordable, compact, research single point diamond turning machine. Proc. ASPE **22**, 184–186 (2000)
18. M. Clarke, M. Pierse, M. Knuefermann, R. Read, New technology and novel design make sub-micron production practical. Proc. ASPE **22**, 187 (2000)
    Micro Contact Printing (μCP)
19. T.E. Creigton, *Proteins: Structures and Molecular Properties* (Freeman, 1985).
20. J.S. Lindsey, Self-assembly in synthetic routes to molecular devices. bio-logical principles and chemical perspectives: a review. New J. Chem. **15**, 153–180 (1991)
21. G.M. Whitesides, E.E. Simanek, J.P. Mathias, C.T. Seto, D. Chin, M. Mammen, D.M. Gordon, Non-covalent synthesis: using physical-organic chemistry to make aggregates. Acc. Chem. Res. **28**, 3744 (1995)
22. N. Bowden, A. Terfort, J. Carbeck, G.M. Whitesides, Self-assembly of mesoscale objects into ordered two-dimensional arrays. Science **276**, 233–235 (1997)
23. A. Terfort, N. Bowden, G.M. Whitesides, Three-dimensional self-assembly of millimetre-scale components. Nature. **386**, 162–164 (1997)
24. Y. Xia, G. Whitesides, Soft lithography. Annu. Rev. Mater. Sci. **28**, 153–184 (1998)
    Replica Moulding (REM) Replica Moulding (REM)
25. D.A. Kiewit, Microtool fabrication by etch pit replication. Rev. Sci. Instrum. **44**, 1741–1742 (1973)
26. M.C. Hutley, *Diffraction Gratings* (Academic, New York, 1982)
27. M. Nakano, N. Nishida, Contact printing method utilizing heated photo-resist adhesive property for hologram copying. Appl. Opt. **18**, 3073–3074 (1979)
    Micro-transfer Moulding (μTM)
28. X.M. Zhao, S.P. Smith, S.J. Waldma, G.M. Whitesides, M. Prentiss, Demonstration of waveguide couplers fabricated using micro-transfer molding. Appl. Phys. Lett. **71**, 1017–1019 (1997)

29. X.M. Zhao, Y. Xia, G.M. Whitesides, Fabrication of three- dimensional micro-structures: Microtransfer molding. Adv. Mater. **8**, 837–840 (1996)
30. O.J.A. Schueller, S.T. Brittain, G.M. Whitesides, Fabrication of glassy carbon microstructures by soft lithography. Sens. Act. A. **72**, 125–139 (1999)
31. C. Marzolin, S.P. Smith, M. Prentiss, G.M. Whitesides, Fabrication of glass microstructures by micro-molding of sol-gel precursors. Adv. Mater. **10**, 571–574 (1998)
    Micro-moulding in Capillaries (MIMIC)
32. M. Trau, N. Yao, E. Kim, Y. Xia, G.M. Whitesides, I.A. Aksay, Microscopic patterning of orientated microscopic silica through guided growth. Nature **390**, 674–676 (1997)
33. E. Kim, Y. Xia, G.M. Whitesides, Micromolding in capillaries: applications in materials science. J. Am. Chem. Soc. **118**, 5722–5731 (1996)
34. E. Delamarche, A. Bernard, H. Schmid, B. Michel, H.A. Biebuyck, Patterned delivery of immuno-globulins to surfaces using micro-fluidic networks. Science **276**, 779–781 (1997)
    Solvent-Assisted Micro-moulding (SAMIM)
35. Y. Xia, G. Whitesides, Soft lithography. Annu. Rev. Mater. Sci. **28**, 153–184 (1998)
    Electro-discharge and Chemical Machining
36. T. Masuzawa, Wire electro-discharge grinding for micro-machining. Ann. CIRP. **34**, 431–434 (1985)
37. P.K. Mishra, *Nonconventional Machining* (Narosa Publishing House, 1997), p. 89.
    Focused Ion Beam
38. A.A. Tseng, Recent developments in micromilling using focused ion beam technology. J. Micromech. Microeng. **14**, R15–R34 (2004)
39. J. Brugger, G. Beljakovic, M. Despont, N.F. de Rooij, P. Vettiger, Silicon micro/nanomechanical device fabrication based on focused ion beam surface modication and KOH etching. Microelectron. Eng. **35**, 401 (1997)
40. B.S.L. Bischoff, J. Teichert, Writing FIB implantation and sub-sequent anisotropic wet chemical etching for fabrication of 3D structures in silicon. Sens. Act. A **61**, 369 (1997)
41. S. Reyntjens, R. Puers, Focused ion beam induced deposition: fabrication of three-dimensional microstructures and youngs modulus of the deposited material. J. Micromech. **10**, 181–188 (2000)
    Laser Ablation/Machining
42. M. Lee, S. Moon, C.P. Hatano, C.P. Grigoropoulos, Ultra-large lateral grain growth by double laser recrystallization of a-Si films. Appl. Phys. A **73**, 317–322 (2001)
43. J. Jiang, C.L. Callender, J.P. Noad, R.B. Walker, S.J. Mihailov, J. Ding, M. Day, All-polymer photonic devices using excimer laser micromachining. IEEE Photonics Technol. Lett. **16**, 2, 509–511 (2002)
44. S.H. Lee, D.A. Dornfeld, "Precision laser deburring and acoustic emission feedback. J. Manuf. Sci. Eng., Trans. ASME **123**(2), 356–364 (2001)
    Stereo-lithography
45. H. Kodama, Automatic method for fabricating a three-dimensional plastic model with photo-hardening polymer. Rev. Sci. Instr. **52**, 1770–1773 (1981)
    Super IH
46. K. Ikuta, S. Maruo, S. Kojima, New micro stereo lithography for freely movable 3d micro structure, in *Proceedings of IEEE International Workshop on Micro Electro Mechanical Systems (MEMS98)* (1998), pp. 290–295
47. S. Kawata, H.B. Sun, T. Tanaka, K. Takada, Finer features for functional microdevices. Nature. **412**, 697–698 (2001)
48. A. Bertsch, S. Jiguet, P. Renaud, Micro-fabrication of ceramic components by micro-stereo-lithography. J. Micromech. Microeng. **14**, 197–203 (2004)
    Laser Engineered Net Shaping (LENS)
49. M.L. Griffith, M.E. Schlienger, C.L. Atwood, J.A. Romero, J.E. Smugeresky, L.D. Harwell, D.L. Greene, Tooling fabrication using laser engineered net shaping. in *ASME International Mechanical Engineering Congress and Exposition* (1996)

50. M.T. Ensz, M.L. Griffith, Critical issues for functionally graded material deposition by laser engineered net shaping (LENS). in *Proceedings of the 2002 MPIF Laser Metal Deposition Conference* (2002)
    Selective Laser Sintering (SLS)
51. Y.P. Kathuria, Microstructuring by selective laser sintering of metallic powder. Surf. Coating Technol. **116–119**, 643–647 (1999)
    Chemical Vapour Deposition (CVD)
52. W.J. Lackey, J.A. Hanigofsky, R.D. Hardin, A. Prasad, Continuous fabrication of sic ⁻ ber tows by chemical vapor deposition. J.Amer. Cer. Soc. 1564–1570 (1995)
53. E.A. Judson, D.N. Hill, R.A. Young, J.R. Cagle, W.J. Lackey, W.B. Carter, E.K. Barefield, An analysis of preferred orientation in yba2cu3o7-x super-conducting lms deposited by CVD on single-crystal and polycrystalline substrates. Powder Diffract. **9**(4), 250–259 (1994)
54. M.J. Shapiro, W.J. Lackey, J.A. Hanigofsky, D.N. Hill, W.B. Carter, E.K. Barefield, Chemical vapor deposition of silver films for super-conducting wire applications. J. Alloy. Comp. **187**, 331–349 (1992)
55. C.R. Stoldt, C. Carraro, W.R. Ashurst, D. Gao, R.T. Howe, R. Maboudian, A low-temperature CVD process for silicon carbide MEMS. Sens. Act. A. **97–98**, 410–415 (2002)
56. W.J. Lackey, S. Vaidyaraman, K.L. More, Laminated c-sic matrix composites produced by CVI. J. Am. Cer. Soc. **80**, 1, 113–116 (1997)
    Laser Chemical Vapour Deposition (LCVD)
57. F. Wallenberger, Inorganic bers and micro-fabricated parts by laser assisted chemical vapor deposition (LCVD): Structures and properties. Ceramics Int. **23**, 119–126 (1997)
58. F. Wallenberger, P. Nordine, M. Boman, Inorganic fibers and microstructures directly from the vapor phase. Comp. Sci. Technol. **51**, 193–212 (1994)
59. J. Maxwell, K. Larsson, M. Boman, P. Hooge, K. Williams, P. Coane, Rapid prototyping of functional three-dimensional microsolenoids and electromagnets by high-pressure laser chemical vapor deposition. Solid Freeform Fabrication 529–536 (1998)
    LIGA
60. J. Mohr, LIGA – a technology for fabricating microstructures and micro-systems. Sensors Mater. **10**, 363–373 (1998)
61. S. Chung, H. Hein, J.M.F.J. Pantenburg, U. Wallrabe, LIGA technology today and its industrial applications. in *Proceedings SPIEs International Conference on Micro-robotics and Micro-assembly*, vol. 4184 (Boston, 2000), pp. 44–55
62. H. Kawakatsu, et al., Millions of cantilevers for atomic force microscopy. Rev. Sci. Instrum. **73**, 1188–1192 (2002)
63. H. Kawakatsu, H. Toshiyoshi, D. Saya, K. Fukushima, H. Fujita, Jpn. J. Appl. Phys. Part 1. **6B**, 3962 (1999)
64. H. Kawakatsu, H. Toshiyoshi, D. Saya, K. Fukushima, H. Fujita, Appl. Surf.Sci. **157**, 320 (2000)
65. H. Kawakatsu, H. Toshiyoshi, D. Saya, K. Fukushima, H. Fujita, J. Vac. Sci. Technol. B. **16**, 607 (2000)
66. D. Saya, K. Fukushima, H. Toshiyoshi, H. Fujita, Hashiguchi, H. Kawakatsu, Jpn. J. Appl. Phys. Part 1. **39**, 3793 (2000)
67. T.D. Stowe et al., Attonewton force detection using ultra thin silicon cantilevers. Appl. Phys. Lett. **71**, 288–290 (1997)
68. Fosein, et al., Fully integrated nanoresonator system with Attogram/Hz mass resolution" IEEE MEMS. 867–870 (2005)
69. T. Thundat, P.I. Oden, N.J. Warmack, Micro cantilever sensors, Micro-Scale Thermo-Phys. Eng. **1**, 185–189 (1997)
70. N.V. Lavrik, P.G. Datskos, Femtogram mass detection using photo-thermally actuated nano-mechanical resonators. Appl. Phys. Lett.**82**, 2697–2699 (2003)
71. C.A. Tipple, N.V. Lavrik, M. Culha, J. Headrick, P. Datskos, M.J. Sepaniak, Nano-structured micro-cantilevers with functionalised cyclodextrine receptor phases: self assembled monolayers and vapour –deposited films. Anal. Chem. **74**, 21568 (2002)

72. A.N. Cleland, M. Roukes, Fabrication of high frequency nano-metre scale mechanical resonators from bulk Si crystals. Appl. Phys. Lett. **69**, 2653–2655, (1996)
73. M. Tortonese, R.C. Barrett, C.F. Quate, Atomic resolution with an atomic force microscope using piezoresistive detection. Appl. Phys. Lett. **62**, 834–836 (1993)
74. J.D. Adams, G. Parrott, C. Bauer, T. Sant, L. Manning, M. Jones, B. Rogers, D. McCorkle, T.L. Ferrell, Nanowatt chemical vapor detection with a self-sensing, piezoelectric microcantilever array. Appl. Phys. Lett. **83**, 3428–3430 (2003)
75. T. GÄoddenhenrich, H. Lemke, U. Hartmann, C. Heiden, Force microscope with capacitive displacement detection. J. Vac. Sci. Tech. A. **8**(1), 383 (1990)
76. G. Neubauer, S.R. Cohen, G.M. McClelland, D. Horn, C.M. Mate, Force microscopy with a bidirectional capacitance sensor. Rev. Sci. Instrum. **61**, 2296–2308 (1990)
77. G. Binnig, H. Rohrer, Scanning tunneling microscopy – from birth to adolescence. Rev. Mod. Phys. **59**(3), 615–630 (1997)
78. G. Binnig, H. Rohrer, C. Gerber, E. Weibel, Tunneling through a controllable vacuum gap. Appl. Phys. Lett. **40**, 178–180 (1982)
79. G. Binning, H. Rohrer, C. Gerber, E. Weibel, Surface studies by scanning tunneling microscopy. Phys. Rev. Lett. **49**, 57–61 (1982)
80. Y. Martin, C.C. Williams, H.K. Wickramasinghe, Atomic force microscopeforce mapping and probing on a sub 100-^{o}A scale. J. Appl. Phys. **61**(10), 4723–4729 (1987)
81. R. Erlandsson, G.M. McClelland, C.M. Mate, S. Chiang, Atomic force microscopy using optical interferometry. J. Vac. Sci. Tech. A. **6**(2), 266–270 (1988)
82. C. SchÄonenberger, S.F. Alvarado, A differential interferometer for force microscopy. Rev. Sci. Instrum. **60**, 3131–3134 (1989)
83. S.R. Mananlis, S.C. Minne, A. Atalar, C.F. Quate, Inter-digital cantilevers for atomic force microscopy. Appl. Phys. Lett. **69**(25), 3944–3946 (1996)
84. G.G. Yaralioglu, A. Atalar, Analysis and design of an inter-digital cantilever as a displacement sensor. J. Appl. Phys. **83**(12), 7405–7415 (1998)
85. B. Ilic, H.G. Craighead, S. Krylove, W. Senaratne, C. Ober and P. Neuzil, Attogram detection using Nano-electromechanical oscillator. J. Appl. Phys. **95**, 3694 (2004)
86. H. Craighead, Attogram detection using nano-electromechanical oscillators, *American Physical Society Meeting* 21–25, 2005
87. B. Ilic, Y. Yang, H.G. Craighead, Virus detection using nanoelectromechanical devices. Appl. Phys. Lett. **85**, 2604–2606 (2004)
88. S.S. Verbridge, J.M. Parpia, R.B. Reichenbach, L.M. Bellan, H.G. Craighead, High quality factor resonance at room temperature with nanostrings under high tensile stress. J. Appl. Phys. **99**, 124304–124304–8 (2006)
89. B. Lassagne, D. Garcia-Sanchez, A. Aguasca y, A. Bachtold, Ultra sensitive mass sensing with a nanotube electromechanical resonator. Nano Lett. **8**(11), 3735–3738 (2008)
90. Y.T. Yang, C. Callegiri, X.L. Feng, K.L. Ekinci, M.L. Roukes, Zeptogram-Scale nanomechanical mass sensing. Nano Lett. **6**(4), 583–586(2006)
91. K. Jensen, K. Kim, A. Zettl, An atomic-resolution nanomechanical mass sensor, Nat. Nanotechnol. **3**, 533–537, (2008).
92. H.B. Peng, C.W. Chang, S. Aloni, T.D. Yuzvinsky, A. Zettl, Ultrahigh frequency nanotube resonators. Phys. Rev. Lett. **97**, 087–203 (2006)
93. X.L. Feng, R.R. He, P.D. Yang, M.L. Roukes, Very high frequency silicon nanowire electromechanical resonator. Nano Lett. **7**, 1953–1959 (2007)
94. H.G. Craighead, S.M. Stavis, K.T. Samiee, Nanodevices for single molecule studies. Control. Nanoscale Motion. **711**, 271–301 (2007)
95. H.J. Mamin, D. Rugar, Sub-attonewton force detection at millikelvin temperatures. Appl. Phys. Lett. **79**, 3358 (2001)
96. T.P. Burg, M. Godin, S.M. Knudsen, W. Shen, G. Carlson, J.S. Foster, K. Babcock, S.R. Manalis, Weighing of biomolecules, single cells and single nanoparticles in fluid. Nature **446**, 1066–1069 (2007)

 97. L.A. Pinnaduwage et al., Use of micro-cantilevers for monitoring of molecular binding to self assembled mono-layers. Langmuir Lett. **19**, 7841–7844 (2003)
 98. B. Rogers, D. York, N. Whisman, M. Jones, K. Murray, J.D. Adams, T. Sulchek, S.C. Minne, Tapping mode atomic force microscopy in liquid with an insulated piezoelectric microactuator. Rev. Sci. Instrum. **73**, 3242–3244 (2003)
 99. J. Colchero, H. Bielefeldt, A. Ruf, M. Hipp, O. Marti, J. Mlynek, Scanning force and friction microscopy. Phys. Stat. Sol. (a). **131**, 73–75 (1992)
100. S.C. Minne, G. Yaralioglu, S.R. Manalis, J.D. Adams, J. Zesch, A. Atalar, C.F. Quate, Automated parallel high speed atomic force microscopy. Appl. Phys. Lett. **72**, 2340–2342 (1998)
101. P.I. Oden, P.G. Datskos, T. Thundat, R.J. Warmack, Un-cooled thermal imaging using a piezoresistive microcantilever. Appl. Phys. Lett. **69**, 21, 3277–3279 (1996)
102. R. Berger, C. Gerber, J.K. Gimzewski, E. Meyer, H.J. GÄuntherodt, Thermal analysis using a micromechanical calorimeter. Appl. Phys. Lett. **69**, pp. 40–42 (1996)
103. J.R. Barnes, R.J. Stephenson, M.E. Welland, C. Gerber, J.K. Gimzewski, Photothermal spectroscopy with femtojoule sensitivity using a micromechanical device. Nature **372**, 79–81 (1994)
104. J.D. Adams, G. Parrott, C. Bauer, T. Sant, L. Manning, M. Jones, B. Rogers, D. McCorkle, T.L. Ferrell, Nanowatt chemical vapour detection with self sensing, piezo-electric microcantileber array. Appl. Phys. Lett. **83**, 3428–3430 (2003)
105. G.Y. Chen, T. Thundat, E.A. Wachter, R.J. Warmack, Adsorption-induced surface stress and its effects on resonance frequency of microcantilevers. J. Appl. Phys. **77**, 3618–3622 (1995)
106. L. Fadel, F. Lochon, I. Dufor, O. Francais, Chemical sensing: millimetre size resonant microcantilevers performance. J. Micromech. Microeng. **14**, S23–S30
107. R. Raiteri, G. Nelles, H.J. Butt, W. Knoll, P. Skladal, Sensing of biological substances based on the bending of microfabricated cantilevers. Letter to the Editor. Sens. Actuators B. **61**, 213–217 (1999)
108. B. Ilic, D. Czaplewski, M. Zalalutdinov, H.G. Craighead, Single cell detection with micromechanical oscillators. J. Vac. Sci. Tech. B. **19**, 2825–2828 (2001)
109. G. Wu, R.H. Datar, K.M. Hansen, T. Thundat, R.J. Cote, A. Majumdar, Bioassay of prostate-specific antigen (PSA) using microcantilevers. Nat. Biotechnol. **19**, 856–860 (2001)
110. R. McKendry, J. Zhang, Y. Arntz, T. Strunz, M. Hegner, H.P. Lang, M.K. Baller, U. Certa, E. Meyer, H.J. GÄuntherodt, C. Gerber, Multiple label-free biodetection and quantitative DNA-binding assays on a nanomechanical cantilever array. Proc. Nat. Acad. Sci. **99**, 9783–9788 (2002)
111. S. Ming, S. Li, V.P. Dravid, Microcantilever resonance based detection with nanoparticles. Appl. Phys. Lett. **82**, 3562–3564 (2003)
112. T. Oliver, X. Bai, W. John, C. James, *Cantilever Based Biological/Chemical Sensors* (University at Albany, SUNY, 2003, March 23)
113. Y. Arntz, et al., Nano-technology. **14**, 86 (2003)
114. N. Ahmed, D.F. Nino, V.T. Moy, Measurement of solution viscosity by atomic force microscopy. Rev. Sci. Instrum. **72**, 2731–2734 (2001)
115. P.I. Oden, G.Y. Chen, R.A. Steele, R.J. Warmack, T. Thundat, Viscous drag measurements utilizing microfabricated cantilevers. Appl. Phys. Lett. **68**, 3814–3816 (1996)
116. S. Boskovic, J.W.M. Chon, P. Mulvaney, J.E. Sader, Rheological measurements using microcantilevers. J. Rheol. **46**, 891–899 (2002)
117. R.G. Rudnitsky, E.M. Chow, T.W. Kenny, Rapid biochemical detection and differentiation with magnetic force microscope cantilever arrays. Sens. Actuators A. **83**, 256–262 (2000)
118. Y.A. Soh, G. Aeppli, C.Y. Kim, N.D. Mathur, M.G. Blamire, Magnetic domain structure and lattice distortions in manganite films under tensile strain. J. Appl. Phys. **93**(10), 8322–8324 (2003)
119. D. Rugar, R. Budakian, H.J. Mamin, B.W. Chui, Manipulation and detection of electron spins by magnetic resonance force microscopy. AIP Con. Proc. **696**(1), 45–52 (2003)

120. H.J. Mamim, Thermal writing using a heated atomic force microscope tip. Appl. Phys. Lett. **69**(3), 433–435 (1996)
121. B.W. Chui, T.D. Stowe, T.W. Kenny, H.J. Mamin, B.D. Terris, D. Rugar, Low-stiffness silicon cantilevers for thermal writing and piezoresistive readback with the atomic force microscope. Appl. Phys.Lett. **69**(18), 2767–2769 (1996)
122. G. Binnig, M. Despont, U. Drechsler, W. HÄaberle, M. Lutwyche, P. Vettiger, H.J. Mamim, B.W. Chui, T.W. Kenny, Ultrahigh-density atomic force microscopy data storage with erase capability. Appl. Phys. Lett. **74**(9), 1329–1331 (1999)
123. P. Vettiger, G. Cross, M. Despont, U. Drechsler, U. DÄurig, B. Gotsmann, W. HÄaberle, M.A. Lantz, H.E. Rothuizen, R. Stutz, G.K. Binnig, The millipede"- nanotechnology entering data storage. IEEE Trans. Nanotechnol. **1**, 1 (2002)